Drug Design, Development and Therapy

Dovepress
Taylor & Francis Group

Open Access Full Text Article

ORIGINAL RESEARCH

Danggui-Shaoyao-San Can Ameliorate Alzheimer's Disease by Inhibiting Hippocampal Neuron Apoptosis: Findings from Serum Pharmacology

Kai-Xin Zhang[1], Ji-Wei Zhang[2], Yan-Hong Jiang[1], Yi-Ran Wang[1], Zhen-Ling Liu[1], Peng-Li Ding[1], Xiang-Ying Wang[1], Wen-Qiang Cui[3], Xiang-Qing Xu[3,*], Ya-Han Wang[3,*]

[1]First College of Clinical Medicine, Shandong University of Traditional Chinese Medicine, Jinan, 250000, People's Republic of China; [2]College of Acupuncture and Massage, Shandong University of Traditional Chinese Medicine, Jinan, 250000, People's Republic of China; [3]Department of Neurology, Affiliated Hospital of Shandong University of Traditional Chinese Medicine, Jinan, 250000, People's Republic of China

*These authors contributed equally to this work

Correspondence: Xiang-Qing Xu, Ya-Han Wang; Department of Neurology, Affiliated Hospital of Shandong University of Traditional Chinese Medicine, Jinan, 250000, People's Republic of China, Email happyxiangqing@163.com; sdwangyahan@sina.com

Background: Danggui-Shaoyao-San (DSS) is a traditional Chinese medicine prescription with a history of nearly 2000 years, originally widely used for gynecological diseases, and in recent years research has found that DSS also has a good therapeutic effect on Alzheimer's disease (AD).

Purpose: The objective is to investigate the metabolic components of the DSS in the blood and the potential mechanisms for AD.

Materials and Methods: Liquid chromatography–mass spectrometry (LC-MS) combined with gas chromatography–mass spectrometry (GC-MS) based non-targeted metabolomics were used to conduct in-depth research. Serum Pharmacology was used to analyze potential mechanisms of DSS for AD. C57BL/6J mice and Hippocampal neuronal cell line (HT-22) were used to prepare the AD model. Enzyme linked immunosorbent assay (Elisa), quantitative polymerase chain reaction (q-PCR), Morris water maze,Western blot (WB), Immunohistochemical and Immunofluorescence were used to study the effect of DSS on AD. Flow cytometry and Cell Counting Kit-8 (CCK-8) reveal the effect of DSS serum on HT-22 proliferation and apoptosis.

Results: A total of 57 metabolic components were screened in DSS serum. Serum Pharmacology revealed that the calcium signaling pathway and cAMP/PKA/CREB pathway may be a potential mechanism through which DSS treated AD. DSS can reduce aberrant phosphorylation of Tau and modulates cAMP/PKA/CREB pathway to improve cognition and apoptosis in AD mice. DSS serum can increase the cell viability of HT-22 and reduce apoptosis mainly by alleviating mitochondrial calcium overloading.

Conclusion: DSS can modulate the calcium signaling pathway and enhance the cAMP/PKA/CREB signaling pathway to ameliorate Tau aberrant phosphorylation, cognitive deficits and neuronal apoptosis after AD.

Keywords: Alzheimer's disease, calcium signaling pathway, cAMP/PKA/CREB signaling pathway, Danggui-Shaoyao-San, apoptosis, serum pharmacology

Introduction

Roughly 90% of cases of dementia are caused by the progressive neurodegenerative disease Alzheimer's disease (AD).[1] AD includes familial AD and sporadic AD, the latter of which is characterized by a high incidence and complex mechanisms.[1] De la Monte et al first proposed that AD, also known as type 3 diabetes mellitus (T3DM), is a metabolic disease with central insulin resistance as the main manifestation, which is not accompanied by increased peripheral blood glucose levels.[2] DSS is a formula consisting mainly of the following Chinese medicines: *Angelica sinensis (Oliv)., Ligusticum chuanxiong Hort (Umbelliferae), Paeonia lactiflora Pall (Paeoniaceae), Poria cocos (Schw)., Alisma orientalis (Sam)., and Atractylodes macrocephala Koidz (Compositae)*. Gynecological disorders were traditionally

Received: 9 October 2024
Accepted: 15 January 2025
Published: 10 February 2025

Graphical Abstract

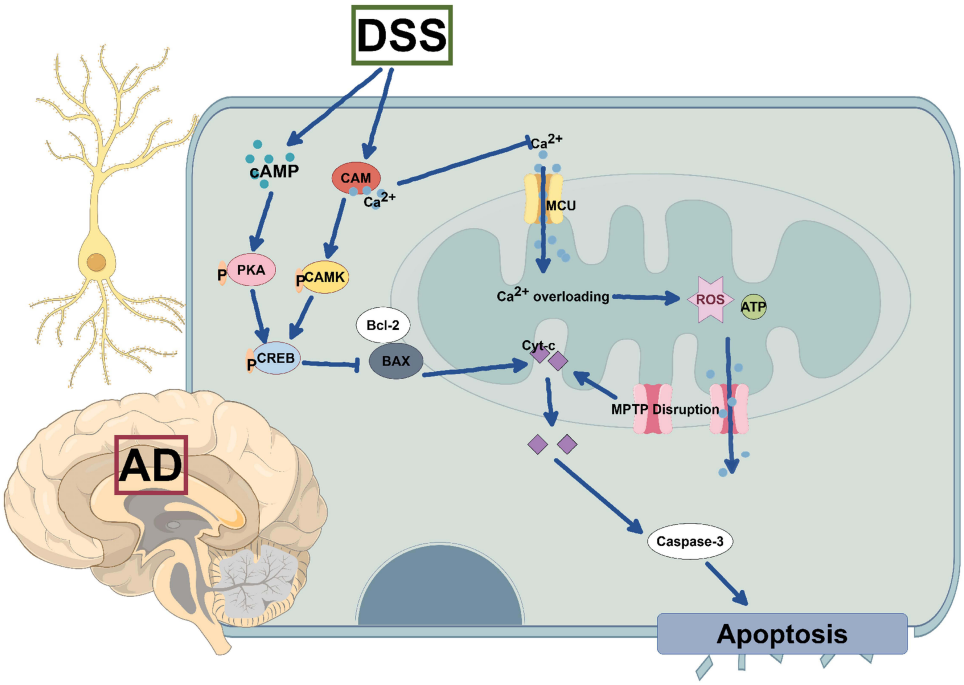

treated with DSS.[3] The use of DSS has been beneficial in enhancing AD patients' quality of life and controlling changes in mood or personality,[4] and has become a hot topic in AD treatment research in recent years.[5,6]

However, based on the view that most drugs only play a role after absorption into the blood, serum medicinal chemistry has become one of the methods with a scientific basis and there has been rapid development of pharmacodynamic substances in recent years.[7] The content of traditional Chinese medicine serums or liquids has been examined in earlier studies, but it ignored the changes before and after the metabolism of drugs into the blood.[8] Therefore, we conducted metabolomic studies on a compound solution of traditional Chinese medicine, the serum of normal mice, and the serum of mice after taking the drug. We conducted in-depth research on the components of DSS compounds and their metabolism after entering the blood using LC–MS combined with GC–MS technology. We used non-targeted metabolomics, serum pharmacology, and network pharmacology to extract the drug components after entry of DSS into the blood, and analyzed the possible mechanism of DSS treatment of AD.

Materials and Methods

Animals

The experimental animals were SPF-grade 6-week-old male C57BL/6J mice(20–25g) (Beijing Vital River Laboratory Animal Technology Co., Ltd.,SCXK[Zhejiang]2021–0006). Use a brain stereotaxic device to position the hippocampus 1.5 mm posterior to the anterior fontanelle and 1.5 mm from the sagittal suture. Insert the microsyringe vertically into 2 mm and inject for 5 min. Control group mice are injected with 5 μL of saline on day 1 and day 3, respectively. The AD model group and the DSS group are injected with 5 μL of streptozotocin (STZ) solution (prepared with saline, 0.3 mg/kg).[9] Mice are anesthetized with continuous inhalation using isoflurane. The animals were raised for 4 months under standard temperature and humidity, lighting during the day, in the SPF animal feeding room (license number: SYXK[Lu]20220009). The European Community guidelines (EEC) provide internationally accepted principles for the use and care of laboratory animals, and this research was carried out in compliance with them. This study has been approved by the

Experimental Animal Ethics Committee of Shandong University of Traditional Chinese Medicine (SDUTEM20230407002).

Cells

The experimental cells were HT22(CL-0595),purchased from procell (Wuhan, China). HT-22 cells were cultured in an incubator with 5% CO_2 and 37°C (Dulbecco's modified eagle medium [DMEM] containing 10% Fetal bovine serum and 1% penicillin streptomycin). Cells were passaged every 24 h (cell density reached 80–90%), and third-generation cells were tested. A simulated in-vitro AD model was prepared by treating HT-22 cells with 10 mm streptozotocin (STZ) (HY-13753, MCE)[10]. The MCU is blocked by treating HT-22 cells with 10μM MCUi4(HY-138620, MCE).[11] Cells were divided into five groups: HT-22 (H), HT-22+STZ (S), HT-22+STZ+DSS (D),HT-22+STZ +MCUi4(M), HT-22+STZ +DSS+MCUi4 (D+M).

DSS Serum Preparation

For preparation of DSS liquid, the herbal medicine granules (production batch number: 2209040351) were purchased from the Affiliated Hospital of Shandong University of Chinese Medicine. Chinese medicine granules were dried at room temperature and stored away from light. The drugs were concentrated to 0.927 g/mL by boiling them in double-distilled water and then kept at 4 °C for storage. Sixty adult male mouses were split into two groups at random: the DSS (D) group (n = 30) and the normal (N) group (n = 30). The adult (70 kg) equivalent dose was used for gavage in the D group, and the N group was irrigated with equal volume of double distilled water and gavaged once a day at 8 a.m. for seven consecutive days. Then the mouses were given an intraperitoneal dose of pentobarbital sodium to induce anesthesia, fixed on the experimental bench, and fully exposed to the chest and abdomen. The abdomen was cut with surgical scissors, the abdominal aorta was exposed, and a disposable lancet and vacuum blood collection tube were used to collect blood, the tube was allowed to centrifuge at 3500 rpm for 10 min to separate the serum(frozen at −80 °C).

Mass Spectrometry Analysis

Three samples of DSS liquid were selected. Serum was divided into eight samples from the D (n = 8,D1–D8) and N (n = 8,N1–N8) groups. To assess the stability of the mass spectrometry instrument, a small amount of serum from each of the D and N groups was combined and split into three Quality Control (QC) samples (QC1-QC3). Metabolic profiles in both ESI-positive and ESI-negative ion modes were analyzed using an ACQUITY UPLC I-Class system (Waters Corporation, Milford, USA) in conjunction with a VION IMS QTOF mass spectrometer (Waters Corporation).

The original data were processed using the metabonomics processing software Progenisis QI v3.0 (Nonlinear Dynamics, Newcastle, UK). Qualitative analysis was carried out utilizing The Human Metabolome Database, Lipidmaps (v2.3), METLIN database, and EMDB2.0. Compounds were identified based on the precise mass number, secondary fragments, and isotope distribution. EMDB2.0 is a local mass spectrometry database established by Luming Biological through standardized methods and based on standards. Because there are many databases used for qualitative analysis, many of the metabolic components are obtained, many of which are of little significance for treatment. The components of the traditional Chinese medicine solution were searched and compared to the Traditional Chinese Medicine Systems Pharmacology Database and Analysis Platform (TCMSP, https://old.tcmsp-e.com/tcmsp.php), and the components of DSS were screened out.

Serum Differential Metabolites

We used principal component analysis (PCA) on quality control (QC) samples to assess the stability of the mass spectrometry equipment. In parallel, the properties, consistency, and intra-group repeatability of the metabolite abundance distribution in every sample were assessed using boxplot and hierarchical clustering. Spectral overlap comparisons were also performed on the total ion current (TIC) patterns of the QC samples to assess the instrumental error throughout the experiment. To look for difference metabolites between the N and D groups, multivariate statistical and univariate analyses were employed. The general distribution across samples and the stability of the entire analytic process were observed using unsupervised PCA. Supervised partial least squares analysis (PLS-DA) and orthogonal partial least

squares analysis (OPLS-DA) were then used to determine the differential metabolites and determine the overall differences in metabolic profiles between the groups. The Student's *t*-test was primarily utilized in univariate analysis to compare metabolites between the two groups. The impact and explanatory power of each metabolite's expression pattern on the classification and discrimination of each group were assessed using the variable important in projection (VIP) in the OPLS-DA analysis. The significance of different metabolites between groups was verified as well using the *t*-test. VIP values of the OPLS-DA model's first principal component >1 and *p*-values less than 0.05 were the screening criteria.

Network Pharmacology

The TCMSP database was retrieved to search for protein targets related to the chemical composition of DSS serum, and the UniProt database was used to search for gene names. Disease targets related to AD were searched for. Data in GeneCards (https://www.genecards.org/) and OMIM (https://mirror.omim.org/) databases was searched for using the keyword "Sporadic Alzheimer's Disease" and duplicate targets, which are known targets for AD, were removed. The target genes for drug-disease intersections were acquired and uploaded to the DAVID database for Kyoto Encyclopedia of Genes and Genomes (KEGG) pathway analysis and enrichment analysis of Gene Ontology (GO) biological processes. We used $P \leq 0.05$ as the screening criterion for the obtained data, and the data were visualized using charts.

Morris water maze

The Morris water maze[12] was used to detect spatial learning and memory in mice. The pool is divided into four quadrants, each with different markings on the walls, the water is dyed white with milk powder, and the water temperature is (22±2°C). During the four-day positioning-navigation test, the transparent platform was placed in the first quadrant 1 cm below the surface of the water. During the 3-day study period, the mice are placed on the platform for 10 second to memorize, and then the mice are placed in water from the second and third quadrants (marker-facing), respectively, to record the distance and time (latency) before the mice find the platform. If the platform is not found within 60 second, record as 60 second, pick up the mouse and place it on the platform again for 5 second to learn. The fourth day is the trial period, where mice are placed directly into the water from the second and third quadrants with no memory training.

Cell Counting Kit-8

The concentration of DSS serum was determined by CCK-8. HT-22 was collected in the logarithmic growth phase, after preparing the cell suspension and adjusting the cell density to 1.0×10^4 / mL, the cells were inoculated in 96-well plates (100 μL/well). According to the DSS serum concentration, the cells were divided into 0, 5, 10, 15, 20, 25, and 30% with six replicated wells per group. A blank group was established with only medium (ie, no cells), with a total of eight groups. After the cells are adherent and the growth state is well, the waste solution is discarded, and different concentrations of DSS serum medium are added at 100 μL/well (DSS serum is dissolved in the medium containing fetal bovine serum). Normal (N) and DSS serum (DSS) groups were set in the same way to observe the safety and effect of normal mouse serum and DSS serum on normal HT-22. Based on the methods of the previous two groups of experiments, we set the normal group serum + STZ group (N + STZ) and the DSS serum + STZ group (DSS+STZ). Ten mM of STZ solution was added according to the rate of 100 μL/well (ie, STZ was dissolved in the medium of different concentrations of serum of the N and DSS groups). After 24 h, 10 μL of CCK-8 solution was added into each well, followed by a 2-hour dark incubation period. The cell survival rate was then computed using the absorbance value (optical density [OD] value) of each well, which was obtained using a microplate reader operating at 450 nm.

Enzyme-Linked Immunosorbent Assay

Intracellular cAMP was measured by ELISA. cAMP ELISA KIT (CEA003Ge) was purchased from Cloud-Clone-Corp. cAMP supernatant was obtained by centrifugation after cell lysis. The assay wells were standard, sample and blank (6 replicate wells in each group), and assay solution A (37°C for 1 h) and assay solution B (37°C for 30 min) were added sequentially. After washing, substrate solution was added to each well and the colour was developed at 37°C under dark

conditions. Finally, a termination solution is added to each well, and the OD value of each well is determined using an enzyme marker at 450 nm. The concentration of the samples was then calculated using the standard curve equation.

Q-PCR

Cells were lysed and added to a DNA removal column. This was then added to an RA adsorption column, followed by deproteinisation, rinsing and elution of the RNA, and centrifugation to obtain all the RNA. Subsequently, first-strand cDNA synthesis was performed to obtain the cDNA product. PCR solutions were prepared with appropriate amounts of forward primer, reverse primer, 2×SYBR qPCR mix, RNase-free H_2O and cDNA. The two-step PCR cycle was as follows: Hold phase: 2–3 min at 94 °C; PCR phase: first step: 10–20 s at 94 °C, first step: 34s at 60 °C, for a total of 40 cycles. The results were analysed by the relative quantitative $2^{-\Delta\Delta CT}$ method. q-PCR experiments were repeated six times independently. Primer information is listed in Table S1.

Immunofluorescence Staining

Each set of cell slides received 50 μL of membrane-breaking working solution, which was then incubated for 20 minutes before the serum was sealed. The tissues were covered with 3% bovine serum albumin(BSA) albumin and sealed for 30 mins. The prepared p-PKA (Abcam,ab32390,1:500) and p-CREB (Abcam,ab32096,1:100) antibodies were added to the well plate at 4 °C for the entire night. Then, the appropriate secondary antibody was incubated. The 4',6-diamidino-2-phenylindole (DAPI) staining solution was added dropwise to re-stain the nuclei incubated in the dark for 10 mins. After washes, a fluorescent microscope was used to take the pictures. ImageJ was used to analyze the relative fluorescence expression (n = 6).

Immunohistochemical Staining

The paraffin sections were sequentially deparaffinized to water, antigenically repaired, endogenous peroxidase blocked, serum blocked, primary antibody added(p-tau, Abcam,ab32057,1:1000; cyt-c,PTG,10993-1-AP,1:500), secondary antibody added, DAB color developed, and nuclei restained. Finally, the sections were dehydrated and sealed for microscopic image acquisition and analysis. Hematoxylin-stained nuclei are blue in color, and the positive expression of DAB is brownish yellow.

Western Blot

Each group of hippocampus and cells was collected separately, total protein was extracted using radio immunoprecipitation assay (RI-PA) cell lysate, and the protein content was determined using the bicinchoninic acid assay (BCA) method. Protein samples were separated by sodium dodecyl sulfate polyacrylamide gel electrophoresis (SDS-PAGE), transferred to PVDF membranes, blocked for two hours with 5% skim milk powder, then incubated with the primary antibody for an entire night. p-tau (Abcam,ab32057,1:1000), tau(Abcam,ab312308,1:1000), p-CaMKII(CST,12716,1:1000), PKA (CST,4782,1:1000), p-PKA(Abcam,ab32390,1:1000), CREB(Abcam,ab32515,1:1000), p-CREB(Abcam, ab32096,1:1000), Bcl-2(Abcam,ab194583,1:1000), BAX(Abcam,ab32503,1:5000), cl-Casepase-3(PTG,19677-1-AP,1:1000), cyt-c(PTG,10993-1-AP,1:5000). Finally, the membranes are then incubated for one hour with secondary antibodies (PTG,SA00001-2,1:1000). Image J was used to analyze the bands(n = 3).

Flow Cytometry

HT-22 apoptosis was assessed by flow cytometry. Annexin V-PE Apoptosis Assay Kit (MA0429, meilune, China). Cell precipitates were resuspended in 400 μL of binding buffer and used for experiments. HT-22 cells were stained with Annexin V-PE and 7-AAD. They were then incubated in the dark for 15 minutes and detected by flow cytometry within 1 hour.

Mitochondrial ROS

ROS expression levels in cellular mitochondria were detected using the Mitochondrial Superoxide Assay Kit (MitoSOX) (Beyotime, S0061S), and experiments were performed according to the instructions.

Calcium Concentration

The calcium concentration was quantified in the cytoplasm utilizing the Fluo-4 Assay Kit (Beyotime, S1061S), while the mitochondrial concentration was determined through the use of Rhod-2, AM (Invitrogen, R1245MP). HT-22 cells were inoculated in 24-well plates, and the cells were washed with PBS once during the experiment. Then 250 μL of Fluo-4 staining solution was added to each well. The cells were incubated at 37°C for 30 minutes in the dark. The staining effect was observed under a fluorescence microscope (Fluo-4 AM exhibits green fluorescence at 490/525 nm). Subsequently, 250 μL of 5 μM Rhod-2 AM was added to the 24-well plates at 37 °C for 30 minutes. Finally, the cells were washed with PBS and observed using a fluorescence microscope (Rhod-2 AM exhibits red fluorescence at 552/581 nm).

Mitochondrial Permeability Transition Pore (MPTP) and Membrane Potential

MPTP was assayed using the MPTP Assay Kit (Beyotime, C2009S); mitochondrial membrane potential was assayed using the JC-1 Kit (Beyotime, C2006). Experiments were carried out according to the instructions.

ATP

Cellular ATP content was measured using an ATP assay kit (Beyotime, S0026B) and experiments were carried out according to the instructions.

Statistical Analyses

GraphPad Prism (version 9.4.1) was used to evaluate intergroup differences. Means ± standard deviation are used to depict the data, and one-way analysis of variance was performed. $P < 0.01$ was defined as more significant, and $P < 0.05$ as statistically significant.

Results

DSS Original Liquid

Three hundred metabolites were identified (Figure 1). Two hundred and fifty-one metabolites were detected by LC–MS, of which 162 were detected in positive mode (Figure 1A and Table S2) and 89 were detected in negative mode (Figure 1B and Table S3). Forty-nine metabolites were detected by GS–MS (Figure 1C and Table S4). All metabolites included 40 classes, of which the top five were carboxylic acids and derivatives (13.33%), organooxygen compounds (12.67%), prenol lipids (10%), benzene and substituted derivatives (7%), and fatty acyls (7%) (Figure 1D).

Metabolomics of Traditional Chinese Medicine Entering the Blood

Qc

The PCA model plots produced by 7-fold cross-validation demonstrate how closely the QC samples are clustered together in both LC-MS and GC-MS, as seen in Figure 2A and D, indicating that the mass spectrometry system is stable and repeatable, and the metabolites of the QC samples are consistent (Figure 2B, and E). There was little difference in QC samples (LC-MS) groups, and between groups D and N, the metabolites differed significantly (Figure 2C). The response intensity and retention time of each chromatographic peak were found to be essentially overlapped when the TIC (GC-MS) of the QC samples was compared with the spectral overlap (Figure 2F). This suggests that the variation brought on by instrument error was minimal throughout the entire experiment.

Multivariate Statistical Analysis

The findings indicated that the coordinate points of groups D and N were far apart (Figure 3A–C and F–H), indicating obvious differences between the samples from the N and D groups. The model has good predictive capability, and that subsequent drug component screening could be conducted. These differential metabolites are intuitively reflected in the

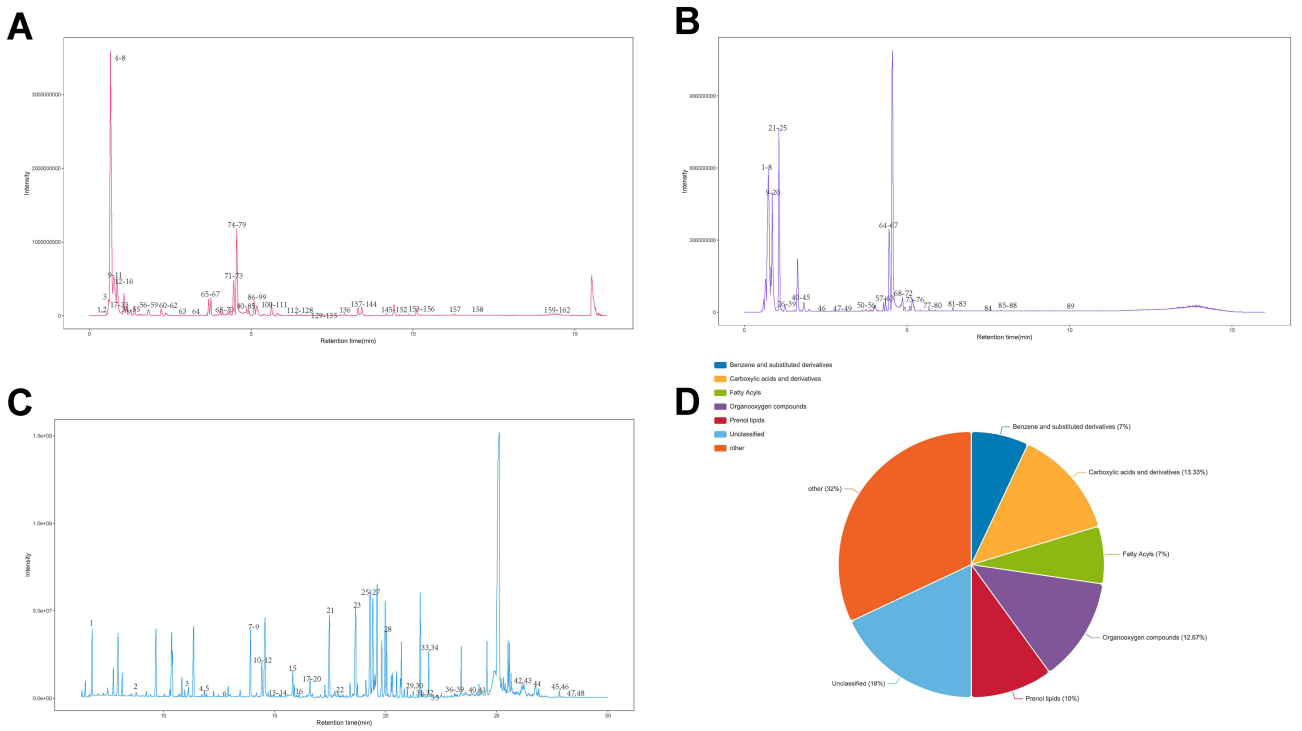

Figure 1 Base peak chromatogram (BPC) and class pie of Danggui-Shaoyao-San original liquid. (**A**) In LC–MS positive ion mode. BPC of all metabolites detected; the abscissa is retention time (min); the ordinate is the mass spectral intensity; and the detected metabolite is marked with a black arrow. (**B**) BPC of all metabolites detected in LC–MS negative ion mode. (**C**) BPC of all metabolites detected in GC–MS. (**D**) Class Pie. LC-MS and GC-MS Classification Pie Chart of All Metabolites Detected in the Pie Chart showing 7 classes: Carboxylic acids and derivatives (13.33%), organooxygen compounds (12.67%), prenol lipids (10%), benzene and substituted derivatives (7%), fatty acyls (7%), unclassified (18%), and other (32%).

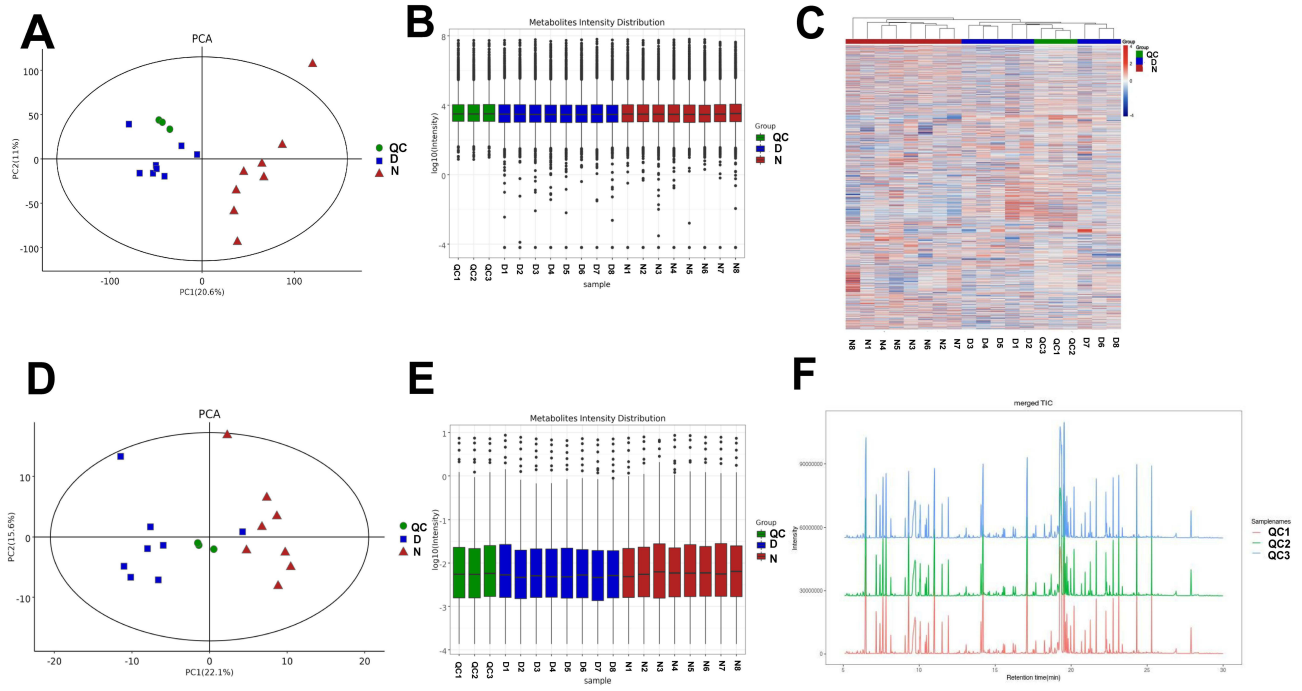

Figure 2 QC. (**A**)PCA(LC-MS). For the first principal component, the interpretation rate is represented by the abscissa PC1, and for the second principal component, by the ordinate PC2. Conversely, the farther the distance between the samples, the greater the difference between the samples. (**B**)Boxplot (LC-MS) of metabolite intensities in QC samples. The sample number is the abscissa, and each metabolite's abundance in the sample is represented by its log10 value on the ordinate. (**C**) Hierarchical clustering of metabolite expressions. Similar samples are grouped together, each column represents a sample, each row represents a metabolite, and the color indicates the relative abundance of metabolites. (**D**)PCA(GC-MS). (**E**)Boxplot (GC-MS) of metabolite intensities in QC samples. (**F**)TIC overlay of QC samples (GC-MS).The abscissa is the retention time (min); the ordinate is the mass spectral intensity.

https://doi.org/10.2147/DDDT.S490900

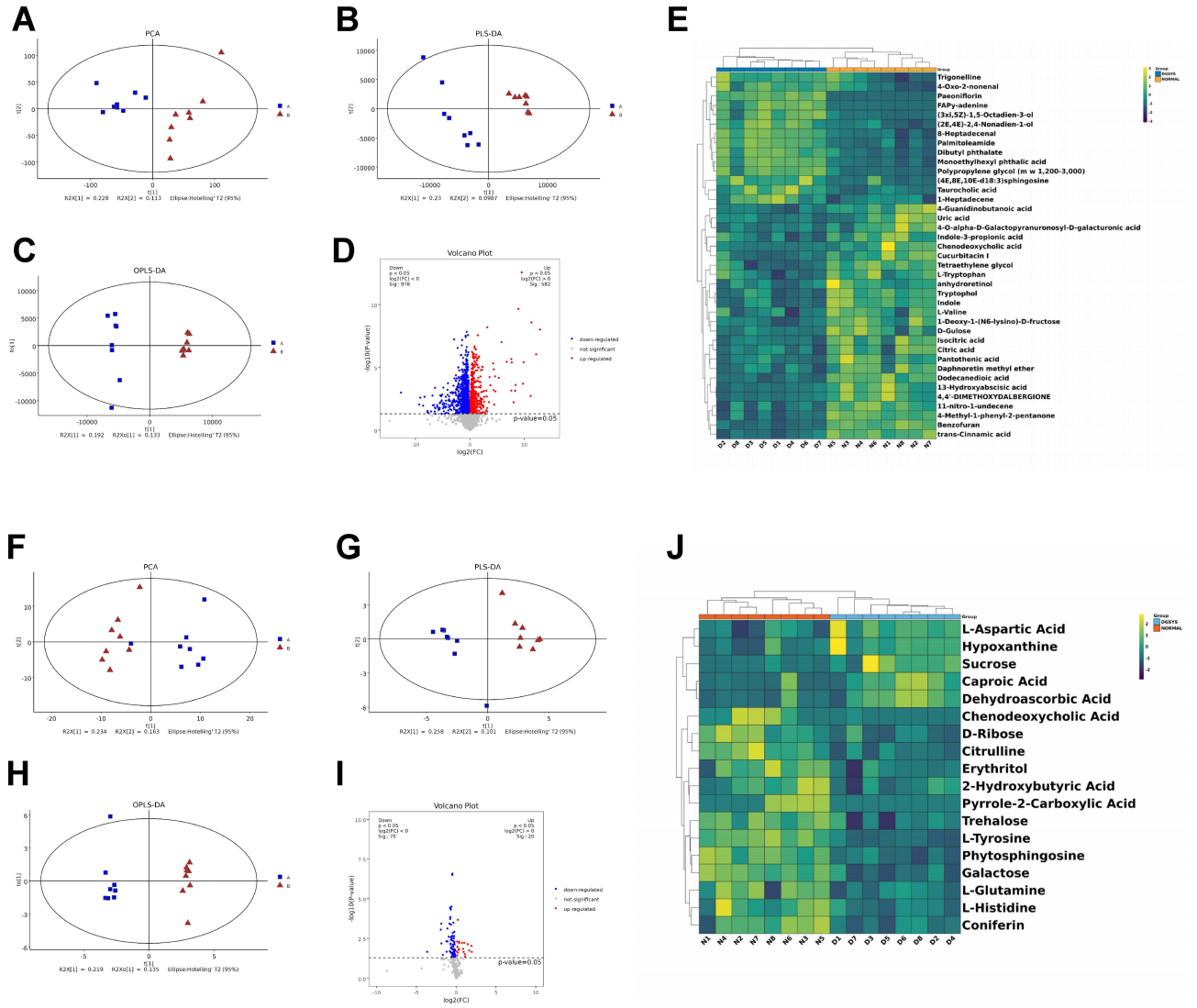

Figure 3 DSS serum multivariate statistical analysis. (**A**) PCA of LC-MS. T[1] and t[2] of this plot represent the score values projected on the PC1 and PC2 for samples, which can intuitively reflect large difference between D and N group samples(95% confidence interval). R2X(cum): reflects the model's cumulative explanatory rate along the X-axis. (**B**) PLS–DA of LC-MS. (**C**) OPLS–DA of LC-MS. (**D**) Volcano plot of LC-MS. The values of the two sets of alignment's log2 (FC) and -log10(p-value) represent the abscissa and ordinate, respectively. Red origin ($P < 0.05$ and FC > 1) represents the metabolite that was upregulated in experimental group, blue origin ($P < 0.05$ and FC < 1) represents the metabolite that was downregulated, and the gray dot represents the insignificant metabolite. (**E**) Clustering heat map of LC–MS. The group is divided into DGSYS (D) and NORMAL (N). The sample name is listed on the abscissa, and the differential metabolite name is listed on the ordinate. The transition from purple to yellow denotes a low to high metabolite expression abundance; that is, the more yellow, the higher the differential metabolite expression. (**F**) PCA of GC–MS. (**G**) PLS–DA of GC-MS. (**H**)OPLS–DA of GC-MS. (**I**) Volcano plot of GC-MS. (**J**)Clustering heat map of GC–MS.

volcano plot (Figure 3D and I), including the significant upregulation and downregulation of the two metabolites. Hierarchical clustering of the expression of significantly different metabolites was done in order to visualize the association and differences in metabolite expression between each sample (Figure 3E and J). In the LC-MS and GC-MS clustering heat maps, the samples from the two groups show notable differences in metabolites.

Serum Traditional Chinese Medicine Components

Fifty-seven metabolites were identified (Figure 4). Thirty-nine metabolites were detected by LC–MS, of which 26 were detected in positive mode (Figure 4A and Table S5) and 13 were detected in negative mode (Figure 4B and Table S6). Eighteen metabolites were detected using GC–MS (Figure 4C and Table S7). All metabolites included 20 classes, of which the top five were organo-oxygen compounds (22.81%), carboxylic acids and derivatives (15.79%), fatty acyls (10.53%), indoles and derivatives (7.02%), and steroids and steroid derivatives (7.02%) (Figure 4D).

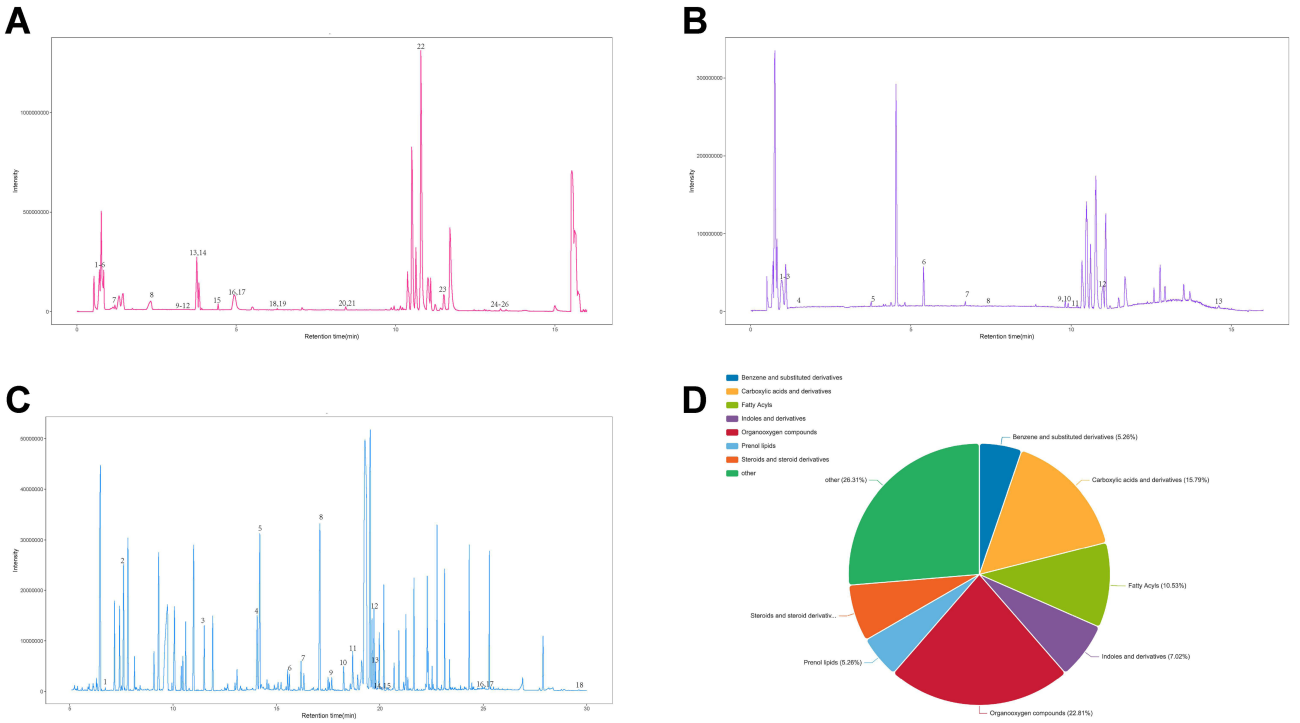

Figure 4 Base peak chromatogram (BPC) and class pie of DSS serum. (**A**) BPC of all metabolites detected by DSS serum in LC–MS positive ion mode. (**B**) BPC of all metabolites detected by DSS serum in LC–MS negative ion mode. (**C**) BPC of all metabolites detected by DSS serum in GC–MS mode. (**D**) Class pie. LC–MS and GC–MS detected DSS serum. All metabolite classification pie chart showing seven classes: Organooxygen compounds (22.81%), carboxylic acids and derivatives (15.79%), fatty acyls (10.53%), indoles and derivatives (7.02%), steroids and steroid derivatives (7.02%), prenol lipids (5.26%), benzene and substituted derivatives (5.26%), and others (26.31%).

Network Pharmacology

A total of 57 serum metabolites were obtained and 97 drug targets were identified. A total of 6585 disease targets for AD and 73 drug ingredient-disease targets were identified(Figure 5A). GO analysis of 73 targets of AD (Figure 5B)showed that the biological processes included the intracellular steroid hormone receptor signaling pathway, drug response, and chemical synaptic transmission. The cellular components included the plasma membrane, membrane rafts, and dendritic spines. Its molecular functions included nuclear receptor activity and enzyme and steroid binding. The KEGG enrichment analysis results of ingredient-disease targets(Figure 5C) showed that the top three environmental information processing pathways were the calcium signaling pathway, neuroactive light receptor interaction, and the AMP signaling pathway. Related studies have confirmed the therapeutic value of the calcium signaling pathway[13,14] and cAMP pathway in AD[15]. Therefore, we choose calcium signaling pathway and cAMP signaling pathway is the cAMP/PKA/CREB pathway for further validation.

DSS Reduces Aberrant Phosphorylation of Tau and Modulates cAMP/PKA/CREB Pathway to Improve Cognition and Apoptosis in AD Mice

The IHC results (Figure 6A and B) revealed aberrant phosphorylation of the Tau protein in the CA1 region of the hippocampus, which is consistent with the typical pathological changes of AD[16], DSS was observed to significantly improve the aberrant phosphorylation of tau ($P < 0.01$). The same results were observed in WB (Figure 6C and D), where p-Tau expression was increased in the hippocampal region of AD model mice ($P < 0.01$), and DSS was found to downregulate p-Tau expression ($P < 0.05$). Subsequently, the cognitive ability of the mice was tested using the Morris water maze. The results (Figure 6E–G) demonstrated that the AD model mice exhibited a longer latency time to find the platform and swam a greater distance than the other two groups ($P < 0.01$). This suggests that the spatial learning and memory ability of the AD model mice was significantly reduced, indicating that DSS can improve the cognitive function of AD mice.

https://doi.org/10.2147/DDDT.S490900

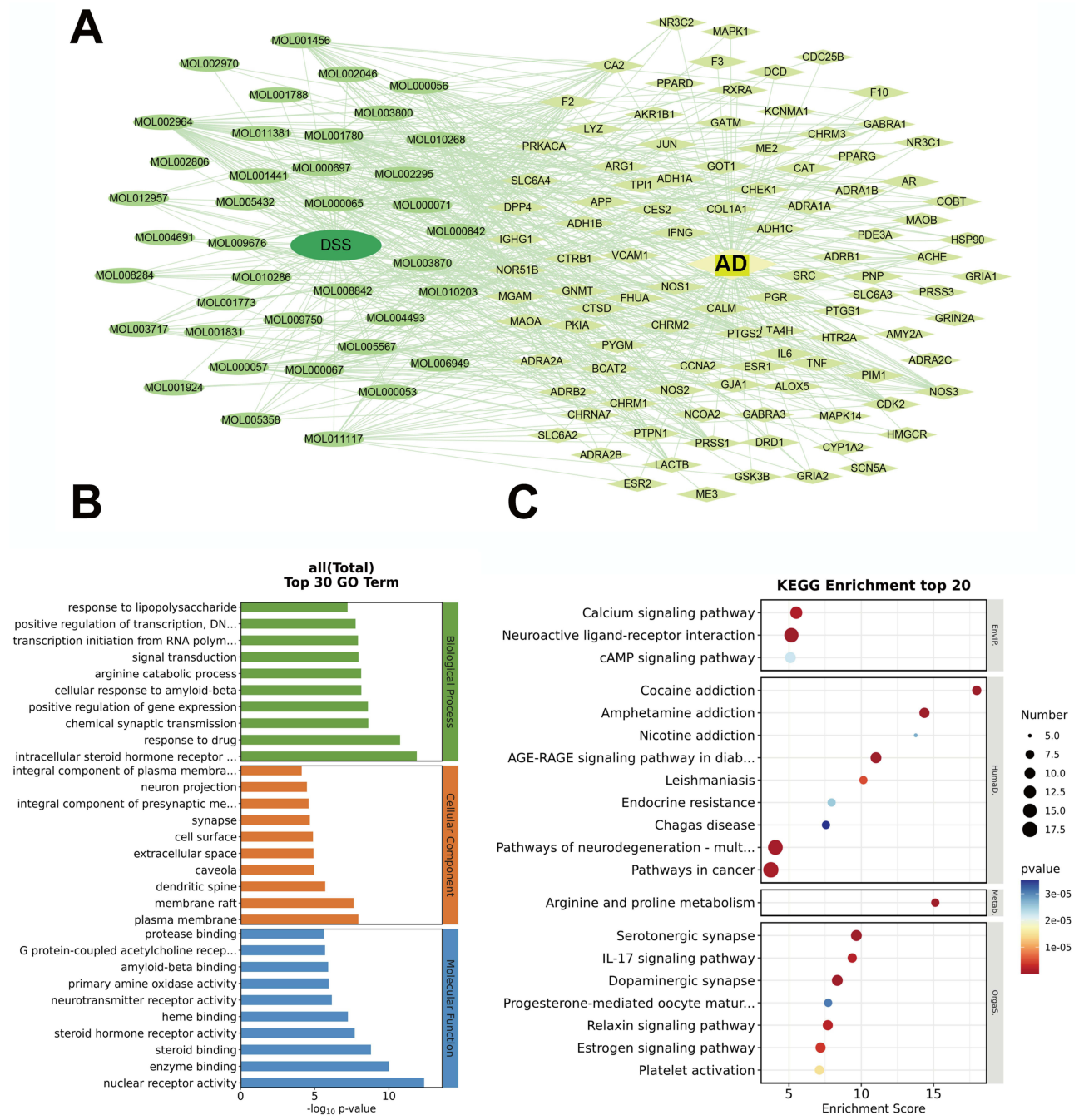

Figure 5 Network pharmacology. (**A**) DSS-AD targets network diagram.(**B**) GO analysis of DSS serum components that may act on targets of AD. The bar chart was displayed according to the 10 items in order from largest to smallest corresponding to the-$\log_{10}$p-value of each entry. (**C**) KEGG enrichment top 20 of DSS serum components that may act on targets of AD.

The results obtained from KEGG analysis were also validated in AD mice, and we found a downregulation of p-CaMKII expression after AD and upregulation after DSS intervention (Figure 6I and K) ($P < 0.01$), which initially revealed the modulatory effect of DSS on the calcium signaling pathway in AD mice.[17] Immediately, we verified the expression of key proteins on the cAMP/PKA/CREB pathway, and DSS could promote the phosphorylation of PKA and CREB (Figure 6L and M) ($P < 0.05$).

Of particular interest was the aberrant expression of cytochrome C observed in the hippocampal CA1 region of AD mice following the injection of STZ into the lateral ventricle (Figure 6H). Furthermore, the WB results indicated an

 https://doi.org/10.2147/DDDT.S490900

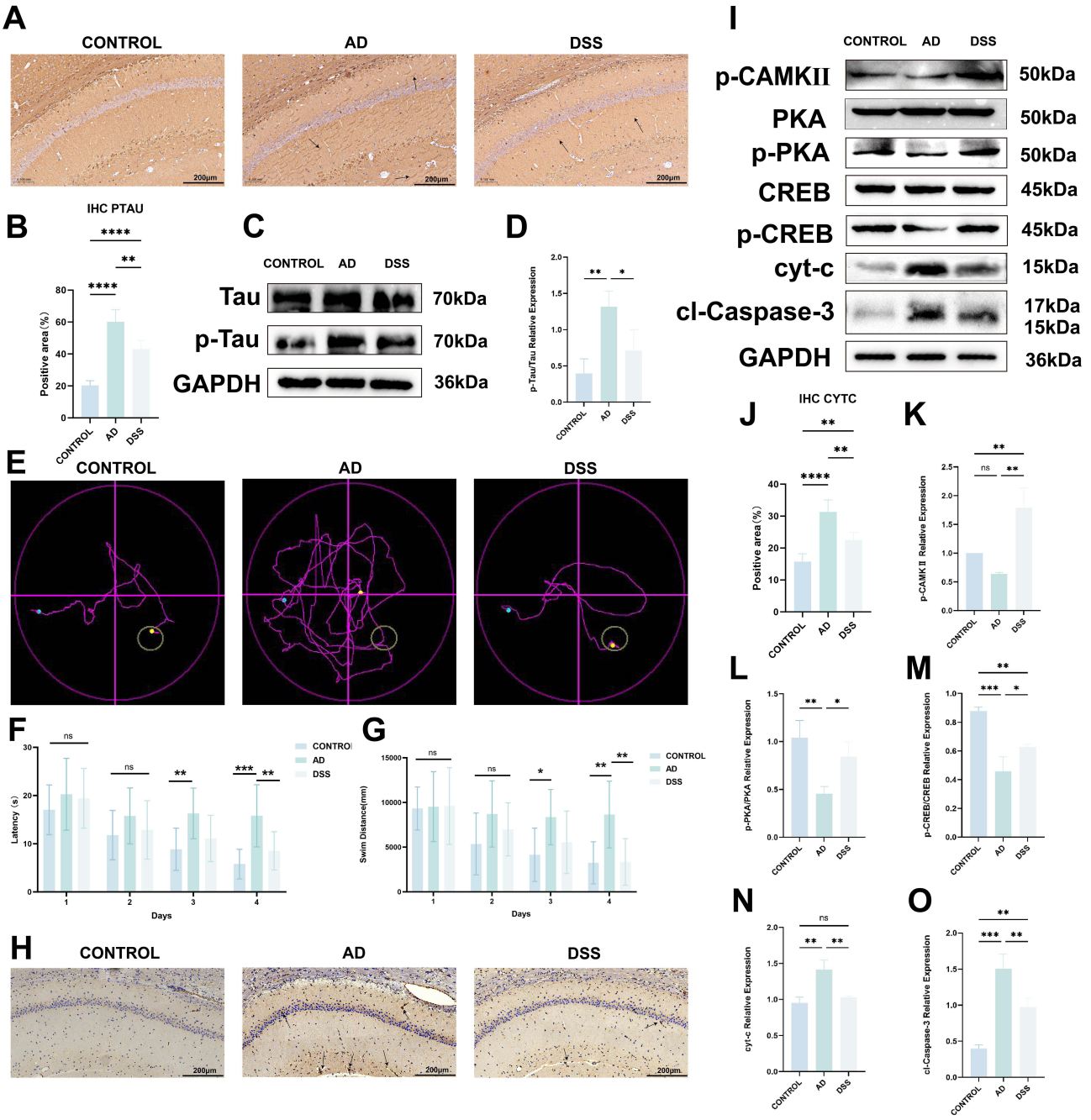

Figure 6 Effects of DSS on AD mice. (**A**) Expression of p-Tau in CA1 region of mouse hippocampus measured by IHC (n = 5).(**B**) Quantitative statistics of p-Tau expression in CA1 region of mouse hippocampus measured by IHC. (**C**) WB results. (**D**) WB results for p-Tau (n = 3). (**E**) Track of Morris water maze. The starting point is between the first and fourth quadrants and the platform is in the third quadrant. (**F**) Latency of Morris water maze (n = 10). (**G**) Swimming distance of Morris water maze (n = 10). (**H**) Expression of cytochrome c in CA1 region of mouse hippocampus measured by IHC (n = 5). (**I**) WB results. (**J**) Quantitative statistics of cytochrome c expression in the CA1 region of mouse hippocampus measured by IHC (n = 5). (**K**) WB results for p-CaMKII (n = 3). (**L**) WB results for p-PKA(n = 3). (**M**) WB results for p-CREB (n = 3). (**N**) WB results for cyt-c (n = 3). (**O**) WB results for cl-Caspase-3 (n = 3). *indicates $P < 0.05$; **indicates $P < 0.01$; *** indicates $P < 0.001$; **** indicates $P < 0.0001$; ns indicates no statistical difference.

increase in the expression of cyt-c and cleaved-caspase 3, which led us to hypothesize that this finding was associated with aberrant apoptosis in neurons following AD. We also postulated that DSS could potentially reduce cyt-c and cleaved-caspase 3 expression ($P < 0.01$), suggesting that DSS may serve as a means of ameliorating the abnormal apoptosis of hippocampal neurons (Figure 6I, N, and O).

https://doi.org/10.2147/DDDT.S490900

DSS Serum Can Increase the Cell Viability of HT-22 Induced by STZ

Serum of the N and DSS groups had the effect of promoting HT-22 growth, and the cell survival rate of the N group continued to increase with the serum concentration increasing, reaching a peak (146.8 ± 32.99%) when the serum concentration reached 20%. The subsequent increase in serum concentration was not significant (Figure 7A). We have observed a similar trend in the DSS group(155.6 ± 47.96%) (Figure 7B). Furthermore, the cell survival rate was slightly higher than that of the N group (Figure 7C and D) (P >0.05). Both groups of serum had a protective effect on HT-22, and the cell survival rate in the N+STZ group increase continuously with the increase of serum concentration, reaching a peak (188.0 ± 63.05%) when the serum concentration reached 15% (Figure 7E). The cell survival rate in the D+STZ group continued to increase with the serum concentration increasing, and the cell survival rate reached a peak (284.8 ± 57.13%) when the serum

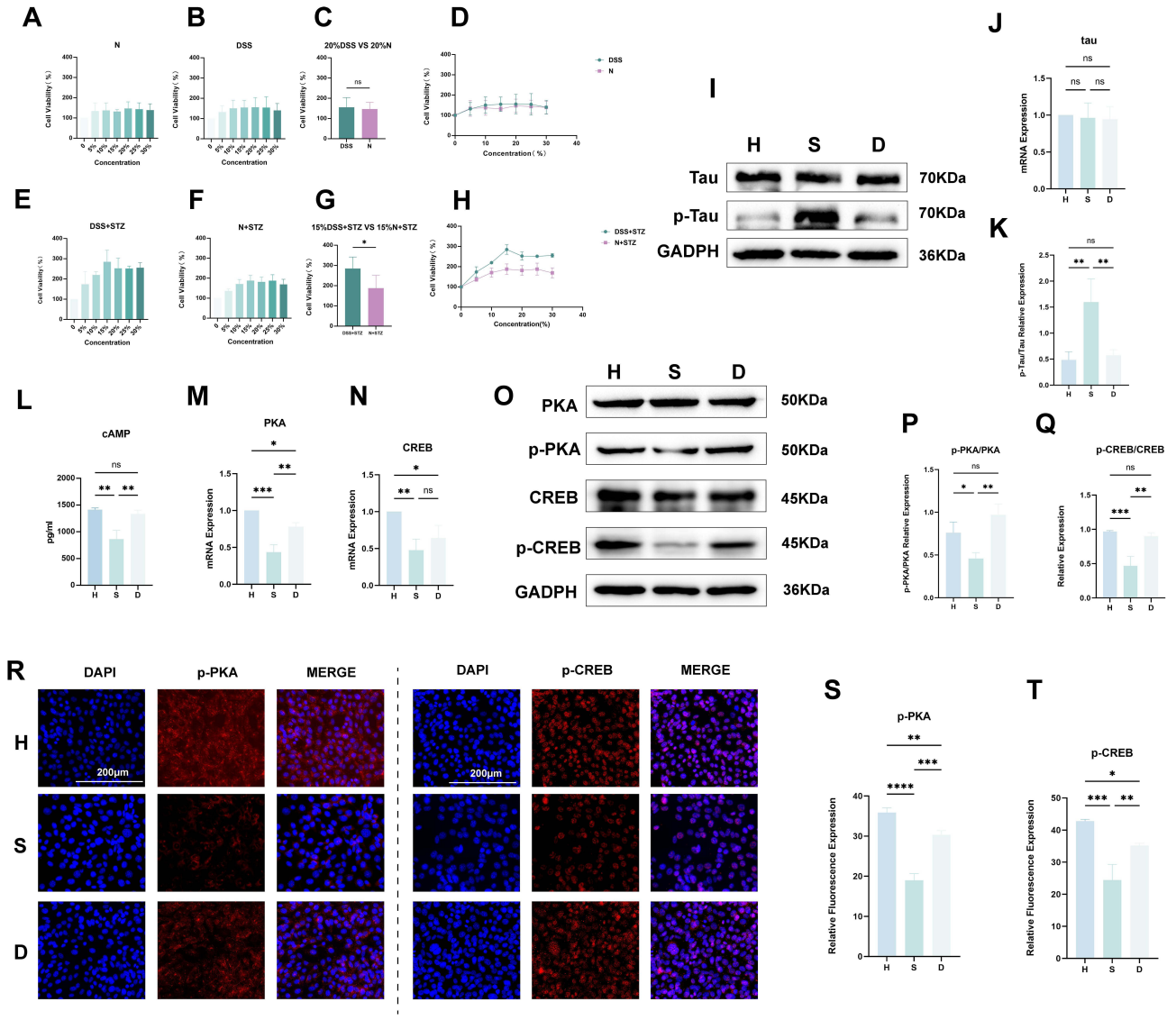

Figure 7 Effect of DSS serum on cAMP/PKA/CREB pathway. (**A**) CCK-8 of HT-22 cells intervened by serum of the N group (n = 6) for 24 h. The abscissa is the serum concentration, which was set to 0, 5, 10, 15, 20, 25, and 30%, and the ordinate is cell viability (%). (**B**) CCK-8 of HT-22 cells intervened by serum of the DSS group (n = 6) for 24 h. (**C**) 20% DSS vs 20% N. (**D**) CCK-8 line plot of HT-22 cells treated with serum from the N and DSS groups (n = 6) for 24 h. (**E**) CCK-8 of HT-22 cells intervened by serum of the N+STZ group (n = 6) for 24 h. (**F**) CCK-8 of HT-22 cells intervened by serum of the DSS+STZ group (n = 6) for 24 h. (**G**) 15% DSS+STZ vs 15% N+STZ. (**H**) CCK-8 line plot of HT-22 cells treated with serum from the N+STZ and DSS+STZ groups for 24 h. (**I**) Results of Western blot (p-Tau). (**J**) q-PCR results of tau mRNA(n = 6). (**K**) Protein expression results of p-tau(n = 3). (**L**) Enzyme linked immunosorbent assay (ELISA) results of cAMP(n = 6). (**M**) q-PCR results of PKA mRNA(n = 6). (**N**) q-PCR results of CREB mRNA(n = 6). (**O**) Results of Western blot. (**P**)Protein expression results of p-PKA(n = 3). (**Q**) Protein expression results of p-CREB(n = 3). (**R**) Immunofluorescence results of PKA. Scale bar=200μm, 63x. (**S**)Fluorescence intensity results of p-PKA(n = 6). (**T**) Fluorescence intensity results of p-CREB(n = 6). *indicates P < 0.05; **indicates P < 0.01; *** indicates P < 0.001; **** indicates P < 0.0001; ns indicates no statistical difference.

https://doi.org/10.2147/DDDT.S490900

concentration reached 15% (Figure 7F), and the cell survival rate was significantly higher than that in the N+STZ group (Figure 7G) ($P < 0.05$). However, the subsequent increase in the serum concentration decreased cell survival (Figure 7H).

DSS Serum Can Reduce Tau Phosphorylation

Furthermore, our findings revealed that the typical pathological alterations associated with AD could manifest within 24 hours following the demise of HT-22 cells induced by STZ. As illustrated in Figure 7J, the tau mRNA expression levels in the H, S, and D groups exhibited no statistically significant difference ($P > 0.05$). Western blot analysis revealed significant intergroup differences in p-tau levels among the H, S, and D groups (Figure 7I and K) ($P < 0.01$). The S group exhibited elevated p-tau expression relative to the H group. The data indicate that DSS reduced tau phosphorylation, as evidenced by the lower p-tau expression in the D group compared to the S group.

Effect of DSS Serum on cAMP/PKA/CREB Pathway

ELISA results showed that cAMP content in cytoplasm of each group was as follows: 1334 ± 69.50 pg/mL (D group), 864.7 ± 163.4 pg/mL (S group), and 1415 ± 31.16 pg/mL (H group) (Figure 7L). Compared to H, the concentration of cAMP in S group was significantly reduced ($P < 0.01$). The D group had a considerably higher quantity of cAMP than the S group ($P < 0.01$), indicating that DSS serum upregulated cAMP and tended to normal levels.

As illustrated in Figure 7M, the S group demonstrated a notable decline in PKA mRNA expression when compared to the H and D groups ($P < 0.05$), as evidenced by the quantitative polymerase chain reaction (q-PCR) data. A notable disparity was discerned in CREB mRNA expression between the H and S groups (Figure 7N) ($P < 0.05$). Western blot analysis (Figure 7O and P) revealed that the level of p-PKA expression was significantly higher in the D group compared to the S group ($P < 0.01$). Additionally, it was observed that the expression of p-CREB in the S group was lower than that in the D group (Figure 7O and Q) ($P < 0.05$). The immunofluorescence results demonstrated that the fluorescence intensity of p-PKA and p-CREB in the H and D groups was higher than that in the S group (Figures 7R–T) ($P < 0.05$).

DSS Serum Can Reduce Apoptosis of HT-22

WB results demonstrated that group S exhibited a significantly higher expression of Bax/Bcl-2 compared to groups H and D (Figure 8A and B) ($P < 0.05$), which suggests that DSS plays a role in counteracting neuronal apoptosis after AD. To confirm that DSS serum reduces apoptosis by affecting p-CaMKII and decreasing the influx of calcium ions into mitochondria, we blocked MCU, the main channel for calcium ion influx into mitochondria, and observed the effects on mitochondria-related apoptotic indexes. Western blot results demonstrated that the expression of p-CaMKII in group S was significantly lower than that of groups H and D after induction by STZ ($P < 0.05$). Furthermore, the use of MCUi4 did not affect p-CaMKII, whereas DSS serum significantly increased the expression of p-CaMKII ($P < 0.05$). In contrast, STZ promoted the expression of cyt-c and cl-caspase-3 in HT-22 cells, thereby increasing the apoptotic rate ($P < 0.01$). Conversely, DSS serum decreased the expression of cyt-c and cl-caspase-3 in HT-22 cells, which resulted in a reduction in the apoptotic rate ($P < 0.05$). Upon blocking MCU, a significant decrease in the expression of cyt-c, cl-caspase-3, and the apoptosis rate was observed ($P < 0.01$), despite the absence of additional improvement with DSS serum (Figure 8C-F, I and J). Furthermore, no significant difference was observed in the expression of MCU itself among the five groups ($P > 0.05$) (Figure 8G and H). It may be postulated that DSS serum up-regulates intracytoplasmic p-CaMKII to promote calmodulin binding to calcium ions and reduces mitochondrial calcium influx to inhibit apoptosis, and that it exerts no effect on calcium influx into the mitochondrial channel MCU.

DSS Reduces Apoptosis Mainly by Alleviating Mitochondrial Calcium Overloading

Our findings revealed that the calcium ion balance in the mitochondria and cytoplasm of HT-22 cells was altered following the induction by STZ. This process involves the influx of calcium ions into the mitochondria and a subsequent decrease in calcium ions in the cytoplasm, ultimately leading to calcium ion overload (Figure 9A and E). This, in turn, promotes the generation of ROS and the depletion of ATP (Figure 9B, F-G, and J ($P < 0.01$), which ultimately results in an increase in mitochondrial membrane permeability and mitochondrial membrane potential (Figure 9C-D, H and I ($P < 0.01$), leading to the release of cyt-c and an increase in the expression of cleaved-caspase-3, thereby inducing apoptosis. This was the antithesis of the effect observed following DSS intervention ($P < 0.01$). Conversely, these conditions ceased to occur

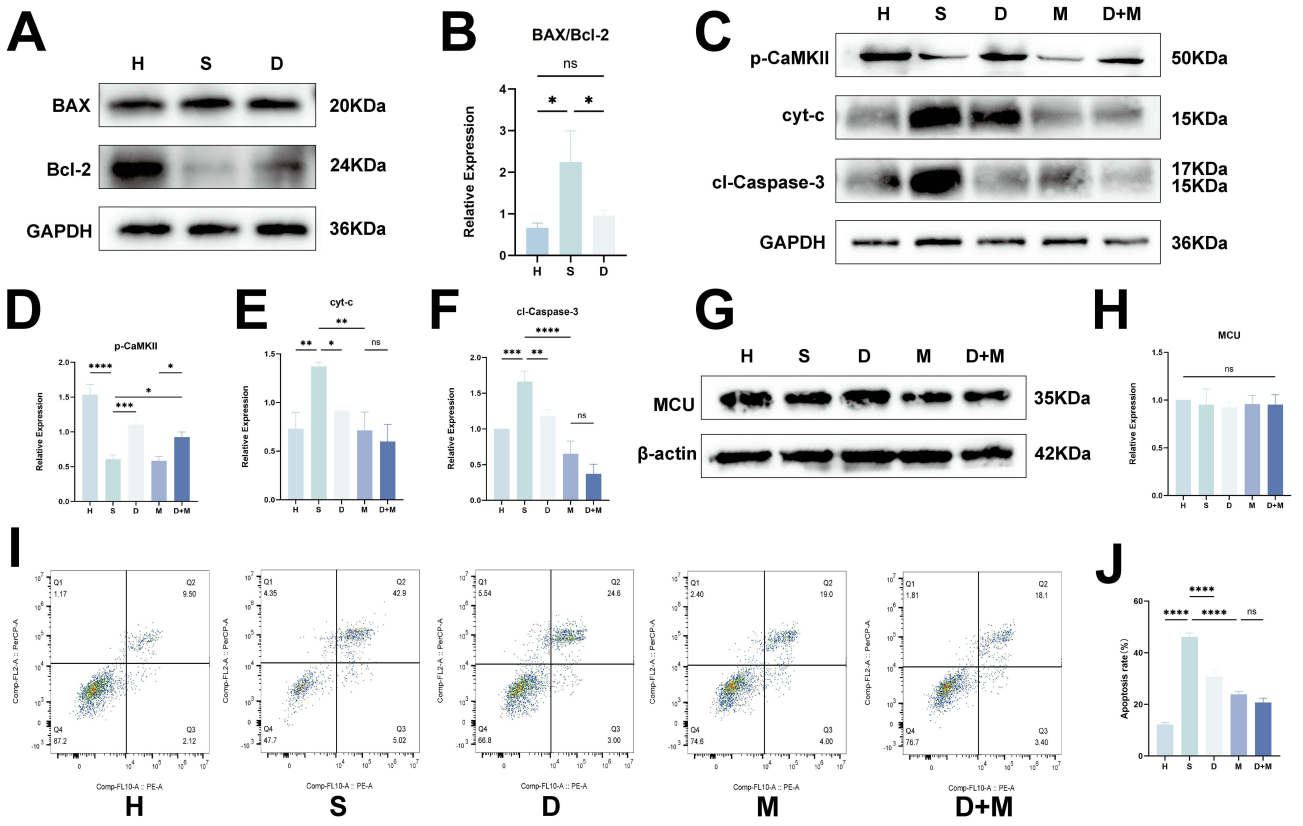

Figure 8 Effect of DSS serum on apoptosis of HT-22. Cells were divided into five groups: HT-22 (H), HT-22+STZ (S), HT-22+STZ+DSS (D),HT-22+STZ +MCUi4(M), HT-22 +STZ+DSS+MCUi4 (D+M). (**A**) Results of Western blot. (**B**) Protein expression results of Bax/Bcl-2(n = 3). (**C**) Results of Western blot. (**D**) Protein expression results of p-CaMKII(n = 3). (**E**) Protein expression results of cyt-c(n = 3). (**F**) Protein expression results of cl-Caspase-3 (n = 3). (**G**) Results of Western blot. (**H**)Protein expression results of MCU (n = 3). (**I**)Apoptosis by flow cytometry. (**J**)Apoptosis rate(n = 3). *indicates $P < 0.05$; **indicates $P < 0.01$; *** indicates $P < 0.001$; **** indicates $P < 0.0001$; ns indicates no statistical difference.

following the blockade of MCU, as evidenced by a review of the preceding results (Figure 8C–F, I and J) ($P < 0.01$). This indirectly confirmed that DSS could up-regulate intracytoplasmic p-CaMKII to promote calmodulin-calcium ion binding and reduce mitochondrial calcium overload to inhibit apoptosis.

Discussion

We detected 300 components in the DSS original liquid and 57 components from the DSS original liquid in the DSS serum, which confirmed that the TCM components were metabolized into the blood. DSS has achieved a certain degree of efficacy in the treatment of AD,[18,19] and previous studies using mass spectrometry have found that the components that play a major role in DSS include ferulic acid, paeoniflorin, and ligustilide, curcumin[20]. Ferulic acid can reverse Aβoligomers-induced morphological defects.[21] Paeoniflorin exert a protective effect on Aβ-induced neurotoxicity[22]. And ligustilide can improve cognitive deficits and the behavioral performance[23]. Curcumin has potential therapeutic value in alleviating symptoms associated with Alzheimer's disease: reduced weight, improved memory function, and regulation of metabolic pathways.[24] Although the therapeutic mechanism has been studied for a long time, the mechanisms of action between components, between targets, and between components and targets, are complex and difficult to explain. Moreover, after oral administration of traditional Chinese medicine liquids into the body, the metabolic process becomes more complicated. In the past, mass spectrometric analysis of Chinese medicinal compounds was often limited to in-vitro drug solutions,[25] which ignored the process of drug metabolism, or were limited to the serum after the drug was metabolized in the blood. The latter method screens out serum differential metabolites in control and drug groups, and it cannot be determined whether all the differential metabolites are derived from the original components of the traditional Chinese medicine. Differential metabolites may contain four parts: the first is the traditional Chinese medicine's active

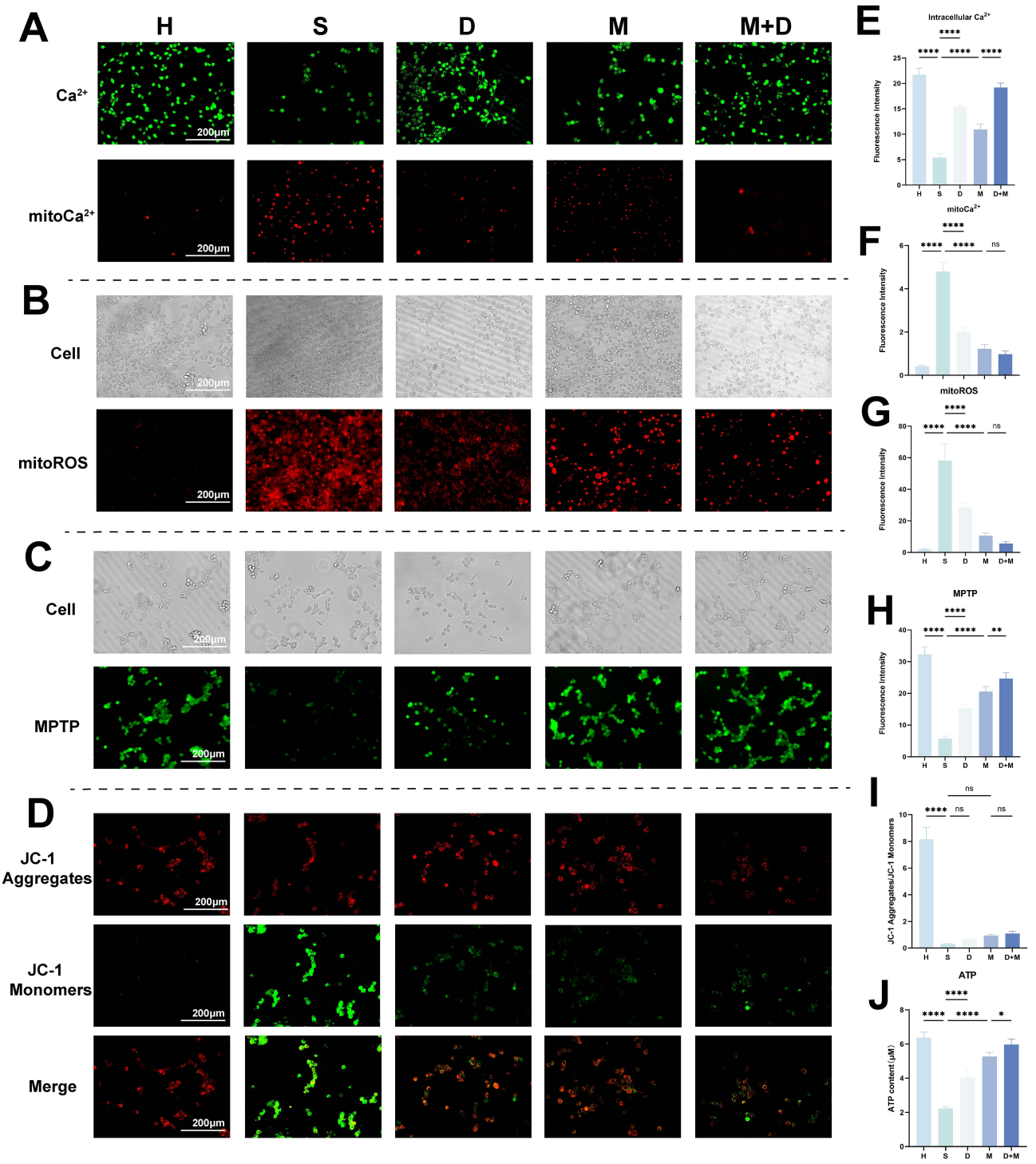

Figure 9 Results of mitochondrial calcium, ROS,MPTP,ATP,membrane potential. (**A**) Results of calcium ions in the cytoplasm versus in the mitochondria (n = 6). (**B**) Results of mitochondrial ROS (n = 6). (**C**) Results of MPTP(n = 6). (**D**) Results of JC-1(n = 6). (**E**) Intracellular calcium ions. (**F**) Mitochondria calcium ions. (**G**) Mitochondria ROS. (**H**) MPTP. (**I**) Mitochondrial JC-1. (**J**) ATP(n = 6). *indicates $P < 0.05$; **indicates $P < 0.01$; *** indicates $P < 0.001$; **** indicates $P < 0.0001$; ns indicates no statistical difference.

component that is directly absorbed into the blood; the second comprises the new components produced after metabolism by the digestive system; the third is the drug components that enter the blood, which participate in and regulate physiological processes and certain metabolic pathways so that the body's original endogenous metabolites are changed

https://doi.org/10.2147/DDDT.S490900

and are reflected in the blood; and the fourth part consists of the widely existing common metabolite components with no therapeutic significance and high abundance.

The results of serum pharmacology suggest that calcium signaling pathway and cAMP/PKA/CREB pathway may be the potential mechanisms of DSS in the treatment of AD. Previous studies have found that calcium ions can act on AD by regulating neuronal apoptosis.[26] Calcium ions bind to calmodulin to form a calcium/calmodulin complex, which activates CaMK and promotes its phosphorylation. Activated CaMK can directly phosphorylate the Ser133 site of CREB and promote its transcriptional activity.[27] When the cell is in a resting state and the concentration of intracytoplasmic calcium ions (Ca^{2+}) is low, MICU1-MICU2 inhibits the entry of Ca^{2+} into the mitochondria through the MCU; whereas when the cell is stimulated and the concentration of intracytoplasmic Ca^{2+} is elevated and exceeds a certain threshold, MICU1-MICU2 allows the entry of Ca^{2+} into the mitochondria through the MCU.[28] Mitochondrial Ca^{2+} overload increases reactive oxygen species (ROS) generation and ATP depletion, which together induce the opening of the MPTP, also known as mitochondrial megachannel (mitochondrial megachannel, MMC). In healthy cells, the inner mitochondrial membrane maintains a normal mitochondrial membrane potential gradient to ensure cellular respiration and energy supply. As Ca^{2+} is taken up and released by mitochondria, the permeability transition pore switches back and forth between open and closed states. The opening of the mitochondrial permeability transition pore significantly alters the permeability of mitochondria. This ultimately led to the release of cytochrome C and the decrease and loss of mitochondrial membrane potential, which in turn activated caspase-9 and caspase-3, leading to apoptosis.[29]

The cAMP/PKA/CREB pathway is a potential target for AD therapy.[30] PKA, which is triggered by cAMP, mediates the many cellular actions of cAMP. This results in the phosphorylation of CREB, which controls cognitive processes and is essential to the development, consolidation, and retrieval of memories.[31] Previous studies on DSS have investigated this mechanism.[32] Recovery from CREB deficiency in the CA1 region of the hippocampus ameliorates synaptic pathology and is associated with cognitive impairment in AD.[33] Additionally, CREB regulates neurogenesis by controlling BDNF expression.[34] CREB phosphorylation mediates consolidation and enhancement of hippocampal synaptic plasticity,[35] and a decrease in CREB phosphorylation and overexpression of Aβ were observed in the brains of AD patients, with Aβ decreasing cAMP levels and PKA phosphorylation events. Aβ reduces the activity of CREB by impairing the activity of BDNF and subsequent inactivation of PKA, and Aβ can also activate GSK3β. Therefore, changes in the cAMP/PKA/CREB signaling pathway mediate the effects of Aβ on hippocampal synaptic loss, synaptic plasticity impairment, and memory problems.[36,37] In addition, CREB examines the integrity of mitochondria by upregulating proteins involved in the protection and preservation of mitochondrial membrane permeability to decrease the amount of cytochrome C released, as this activates caspase- 9.[38] The presence of Bcl-2 and its homologs suggests that mitochondria control the survival and death of cells. PKA and CREB are found in mitochondria and are linked to the development of new behaviors as well as the ability of neurons to withstand a variety of apoptotic stressors by responding to growth factors. Because Bcl-2's promoter region contains an active CRE site, CREB can influence Bcl-2 expression. Additionally, CREB may directly control mitochondrial transcription and modulate neuronal activity.[39]

Abnormal tau phosphorylation is the basic pathological change in AD.[16] Caspase-mediated apoptotic neuronal death is a major cause of AD neuronal loss. Apoptosis in AD involves a conformational change in tau and ultimately promotes filament formation. Aβ also colocalizes with cleaved tau, and this pathway is also affected by caspases. Decreased Bcl-2 levels and increased Bax levels encourage caspase-9 activation, indicating the intrinsic apoptotic mechanism of AD.[38] We found that after STZ-induced, the p-tau levels increased, which preliminarily verified the reliability of the AD model. Furthermore, after application of the DSS serum treatment, the p-tau levels decreased. The CCK-8 results showed that the therapeutic effect of DSS components in the serum, and within a certain concentration range, have obvious protective effect on cells. The optimal serum concentration (15%) can be screened for cell viability. The mechanism by which DSS serum can promote cell proliferation is possibly connected to its apoptosis-inhibiting effect. Subsequent results also confirmed this hypothesis.

The present study demonstrated that DSS directly increased cAMP expression, thereby activating the cAMP/PKA/CREB signaling pathway. This resulted in the activation of downstream PKA and CREB, and ultimately, the phosphorylation of PKA and CREB. Concurrently, DSS has been demonstrated to facilitate the phosphorylation of CaMKII, which suggests that calcium ion binding to calmodulin is augmented and a greater number of calcium/calmodulin complexes are formed. This, in turn, directly promotes the phosphorylation of CREB. DSS increases the phosphorylation of CREB through these two pathways, which has

been demonstrated to be beneficial for the reduction of neuronal apoptosis and the improvement of cognition. In vivo, the Morris water maze indicates that DSS enhances learning capacity and spatial cognition in AD mice. In vitro, DSS was observed to enhance HT-22 survival and mitigate apoptosis. This finding correlates with the established fact that DSS upregulates p-CREB expression, thereby reducing BAX expression, and promotes Bcl-2 expression, which in turn reduces neuronal apoptosis.

DSS upregulated p-CaMKII, which increased the binding of calcium ions to calmodulin, which would decrease the concentration of calcium ions in the cytoplasm and reduce the calcium overload induced by calcium ions entering the mitochondria through the MCU, which in turn reduced the ROS production and ATP depletion, stabilized the MPTP permeability, and reduced the release of cytochrome C and downstream expression of Caspase-3 to inhibit apoptosis. Later, when we blocked MCU, the calcium ions into the mitochondria were reduced, the changes of ROS and ATP in the mitochondria were not significant, and the apoptosis rate of HT-22 was reduced, whereas the effects of both STZ and DSS on MCU were not significant, which proved that both STZ and DSS could affect hippocampal neuron apoptosis through the mitochondrial calcium signaling pathway, and the effects of DSS on other apoptotic pathways were not significant.

Traditional Chinese medicine treatment has rich clinical experience and a unique theoretical system, and has made significant contributions to human health.[40] The use of modern science and technology to research and develop traditional Chinese medicine must focus on its pharmacodynamic material basis. Therefore, studying the basis and mechanism of action of traditional Chinese medicine or compound pharmacodynamic substances has become a focus of academic attention. However, this study only screened out the inherent components of traditional Chinese medicines after entering the blood for mechanistic research, which is inevitably limited. Non-targeted metabolomics mass spectrometry technology can only qualitatively analyze metabolite components and perform enrichment analysis, and cannot quantitatively analyze metabolites. Many components contain a wide range of types, but the content is low and the actual effect is less significant than predicted. The high-abundance components that play the main roles are not screened. Whereas the current work is only a simple validation of the phenotypes of in vivo and in vitro experiments, the specific molecular mechanisms need to be further investigated. Cognitive function and neurobehavior still need more extensive and in-depth studies. These are also the directions for our future efforts.

Conclusion

In the present study, through untargeted metabolomics and serum pharmacology, DSS was found to treat AD by modulating the calcium signaling pathway and enhancing the cAMP/PKA/CREB signaling pathway. The subsequent results provided preliminary evidence that DSS can reduce the aberrant phosphorylation of Tau in the hippocampal CA1 region, ameliorate the cognitive deficits, improve the mitochondrial calcium overload, and inhibit the apoptosis of hippocampal neurons. The current study provides a new rationale for DSS in the treatment of AD.

Abbreviations

DSS, Danggui-Shaoyao-San; QC, Quality Control; ELISA, Enzyme linked immunosorbent assay; GO, Gene ontology; KEGG, Kyoto Encyclopedia of Genes and Genomes; OD, Optical density; OPLS–DA, Orthogonal partial least squares analysis; AD, Alzheimer's disease; PCA, Principal component analysis; PLS–DA, Supervised partial least squares analysis; q-PCR, Quantitative polymerase chain reaction; VIP, Variable important in projection; LC-MS, Liquid chromatography-mass spectrometry combined; GC-MS, Gas chromatography-mass spectrometry; CCK-8, Cell Counting Kit-8; cAMP/PKA/CREB, cyclic adenosine monophosphate/protein kinase A/cAMP-response element binding protein; HT-22, Hippocampal neuronal cell line; STZ, Streptozotocin; p-CREB, phospho-cAMP response element binding; DMEM, Dulbecco's modified eagle medium; TCMSP, Traditional Chinese Medicine Systems Pharmacology Database and Analysis Platform; PBS, Phosphate buffered saline; BSA, Bovine serum albumin; DAPI, 4',6-diamidino-2-phenylindole; RI-PA, Radio immunoprecipitation assay; BCA, Bicinchoninic acid assay; SDS-PAGE, Sodium dodecyl sulfate polyacrylamide gel electrophoresis; PVDF, Polyvinylidene fluoride; TBST, Tris-buffered saline tween-20; ECL, Electrochemiluminescence; BPC, Base peak chromatogram; MCU, Mitochondrial Calcium Uniporter; Ca^{2+}, Calcium ion; CaMKII, Calcium-calmodulin (CaM)-dependent protein kinase II; MPTP, Mitochondrial permeability transition pore.

Acknowledgments

Ya-Han Wang provided financial support to conduct the research. We also thank Hao-Tian Guo and Hong-Wei Zhi for their contributions to the administration of the project. We would also like to thank the Experimental Center, Shandong University of Traditional Chinese Medicine, Jinan 250355, PR China. The Graphical abstract was drawn by Figdraw.

Author Contributions

Kai-Xin Zhang are the first authors. Ya-Han Wang and Xiang-Qing Xu are the corresponding author.

All authors have:

1. Made a significant contribution to the work reported, whether that is in the conception, study design, execution, acquisition of data, analysis and interpretation, or in all these areas.

2. Have drafted or written, or substantially revised or critically reviewed the article.

3. Have agreed on the journal to which the article will be submitted.

4. Reviewed and agreed on all versions of the article before submission, during revision, the final version accepted for publication, and any significant changes introduced at the proofing stage.

5. Agree to take responsibility and be accountable for the contents of the article.

Funding

This work was supported by the Natural Science Foundation of China and the Natural Science Foundation of Shandong Province (grant numbers 82205064 and ZR2021QH110).

Disclosure

The authors report no conflicts of interest in this work.

References

1. Scheltens P, De Strooper B, Kivipelto M. Alzheimer's disease. *Lancet*. 2021;397(10284):1577–1590. doi:10.1016/S0140-6736(20)32205-4
2. Dubois B, Hampel H, Feldman HH, et al. Preclinical Alzheimer's disease: definition, natural history, and diagnostic criteria. *Alzheimer's Dementia*. 2016;12(3):292–323. doi:10.1016/j.jalz.2016.02.002 Proceedings of the Meeting of the International Working Group (IWG) and the American Alzheimer's Association on "The Preclinical State of AD"; Washington DC, USA.
3. Kim M, Kim AR, Park HJ, et al. Danggwijagyaksan for climacteric syndrome in peri- and postmenopausal women with a blood-deficiency dominant pattern: study protocol for a randomized, double-blind, placebo-controlled pilot trial. *Trials*. 2018;19(1):41. doi:10.1186/s13063-018-2443-8
4. Fu X, Wang Q, Wang Z, Kuang H, Jiang P. Danggui-Shaoyao-San: new hope for alzheimer's disease. *Aging Dis*. 2015;7(4):502–513. doi:10.14336/AD.2015.1220
5. Wu Q, Chen Y, Gu Y, et al. Systems pharmacology-based approach to investigate the mechanisms of Danggui-Shaoyao-san prescription for treatment of Alzheimer's disease. *BMC Complement Med Therap*. 2020;20(1):282. doi:10.1186/s12906-020-03066-4
6. Hwang DS, Kim N, Choi JG, Kim HG, Kim H, Oh MS. Dangguijakyak-san ameliorates memory deficits in ovariectomized mice by upregulating hippocampal estrogen synthesis. *BMC Complem Alternat Med*. 2017;17(1):501. doi:10.1186/s12906-017-2015-6
7. Zhang Z, Yi P, Yang J, et al. Integrated network pharmacology analysis and serum metabolomics to reveal the cognitive improvement effect of Bushen Tiansui formula on Alzheimer's disease. *J Ethnopharmacol*. 2020;249:112371. doi:10.1016/j.jep.2019.112371
8. Zhang D, Gou Y, Yu X, et al. Detection and risk assessments of multi-pesticides in Traditional Chinese Medicine Chuanxiong Rhizoma by LC/MS-MS and GC/MS-MS. *Molecules*. 2022;27(3):622. doi:10.3390/molecules27030622
9. Liu S, Fan M, Xu JX, et al. Exosomes derived from bone-marrow mesenchymal stem cells alleviate cognitive decline in AD-like mice by improving BDNF-related neuropathology. *J Neuroinflamm*. 2022;19(1):35. doi:10.1186/s12974-022-02393-2
10. Park J, Won J, Seo J, et al. Streptozotocin induces alzheimer's disease-like pathology in hippocampal neuronal cells via CDK5/Drp1-mediated mitochondrial fragmentation. *Front Cell Neurosci*. 2020;14:235. doi:10.3389/fncel.2020.00235
11. Lan T, Zhang K, Lin F, et al. Effects of MICU1-mediated mitochondrial calcium uptake on energy metabolism and quality of vitrified-thawed mouse metaphase II Oocytes. *Int J Mol Sci*. 2022;23(15):8629. doi:10.3390/ijms23158629
12. Vorhees CV, Williams MT. Morris water maze: procedures for assessing spatial and related forms of learning and memory. *Nat Protocols*. 2006;1(2):848–858. doi:10.1038/nprot.2006.116
13. Chami M. Calcium signalling in alzheimer's disease: from pathophysiological regulation to therapeutic approaches. *Cells*. 2021;10(1):140. doi:10.3390/cells10010140
14. Shah D, Gsell W, Wahis J. Astrocyte calcium dysfunction causes early network hyperactivity in Alzheimer's disease. *Cell Rep*. 2022;40(8):111280. doi:10.1016/j.celrep.2022.111280
15. Delghandi MP, Johannessen M, Moens U. The cAMP signalling pathway activates CREB through PKA, p38 and MSK1 in NIH 3T3 cells. *Cell Signalling*. 2005;17(11):1343–1351. doi:10.1016/j.cellsig.2005.02.003

16. Fortea J, Vilaplana E, Carmona-Iragui M. Clinical and biomarker changes of Alzheimer's disease in adults with Down syndrome: a cross-sectional study. *Lancet*. 2020;395(10242):1988–1997. doi:10.1016/S0140-6736(20)30689-9
17. Yasuda R, Hayashi Y, Hell JW. CaMKII: a central molecular organizer of synaptic plasticity, learning and memory. *Nat Rev Neurosci*. 2022;23:666–682. doi:10.1038/s41583-022-00624-2
18. Liu P, Zhou X, Zhang H, et al. Danggui-Shaoyao-San attenuates cognitive impairment via the microbiota-gut-brain axis with regulation of lipid metabolism in scopolamine-induced amnesia. *Front Immunol*. 2022;13:796542. doi:10.3389/fimmu.2022.796542
19. Hua YQ, Su SL, Duan JA, Wang QJ, Lu Y, Chen L. Danggui-Shaoyao-San, a traditional Chinese prescription, suppresses PGF2alpha production in endometrial epithelial cells by inhibiting COX-2 expression and activity. *Phytomedicine*. 2008;15(12):1046–1052. doi:10.1016/j.phymed.2008.06.010
20. Chen L, Qi J, Chang YX, Zhu D, Yu B. Identification and determination of the major constituents in traditional Chinese medicinal formula Danggui-Shaoyao-San by HPLC-DAD-ESI-MS/MS. *J Pharmaceut Biomed Anal*. 2009;50(2):127–137. doi:10.1016/j.jpba.2009.03.039
21. Picone P, Nuzzo D, Di Carlo M. Ferulic acid: a natural antioxidant against oxidative stress induced by oligomeric A-beta on sea urchin embryo. *Biol Bull*. 2013;224(1):18–28. doi:10.1086/BBLv224n1p18
22. Zhong SZ, Ge QH, Li Q, Qu R, Ma SP. Peoniflorin attentuates Abeta((1-42))-mediated neurotoxicity by regulating calcium homeostasis and ameliorating oxidative stress in hippocampus of rats. *J Neurol Sci*. 2009;280(1–2):71–78. doi:10.1016/j.jns.2009.01.027
23. Wu XM, Qian ZM, Zhu L, et al. Neuroprotective effect of ligustilide against ischaemia-reperfusion injury via up-regulation of erythropoietin and down-regulation of RTP801. *Br J Pharmacol*. 2011;164(2):332–343. doi:10.1111/j.1476-5381.2011.01337.x
24. Lamichhane G, Liu J, Lee S-J, Lee D-Y, Zhang G, Kim Y. Curcumin mitigates the high-fat high-sugar diet-induced impairment of spatial memory, hepatic metabolism, and the alteration of the gut microbiome in alzheimer's disease-induced (3xTg-AD) mice. *Nutrients*. 2024;16(2):240. doi:10.3390/nu16020240
25. Wang ZY, Chu FH, Gu NN, et al. Integrated strategy of LC-MS and network pharmacology for predicting active constituents and pharmacological mechanisms of Ranunculus japonicus Thunb. for treating rheumatoid arthritis. *J Ethnopharmacol*. 2021;271:113818. doi:10.1016/j.jep.2021.113818
26. Sałaciak K, Koszałka A, Żmudzka E, Pytka K. The calcium/calmodulin-dependent kinases II and IV as therapeutic targets in neurodegenerative and neuropsychiatric disorders. *Int J mol Sci*. 2021;22(9):4307. doi:10.3390/ijms22094307
27. Sun P, Enslen H, Myung PS, Maurer RA. Differential activation of CREB by Ca2+/calmodulin-dependent protein kinases type II and type IV involves phosphorylation of a site that negatively regulates activity. *Genes Dev*. 1994;8(21):2527–2539. doi:10.1101/gad.8.21.2527
28. Di Marco G, Vallese F, Jourde B, et al. A high-throughput screening identifies MICU1 targeting compounds. *Cell Rep*. 2020;30(7):2321–2331.e6. doi:10.1016/j.celrep.2020.01.081
29. Rizzuto R, De Stefani D, Raffaello A, Mammucari C. Mitochondria as sensors and regulators of calcium signalling. *Nat Rev Mol Cell Biol*. 2012;13(9):566–578. doi:10.1038/nrm3412
30. Guan R, Lv J, Xiao F, Tu Y, Xie Y, Li L. Potential role of the cAMP/PKA/CREB signalling pathway in hypoxic preconditioning and effect on propofol-induced neurotoxicity in the hippocampus of neonatal rats. *Mol Med Rep*. 2019;20(2):1837–1845. doi:10.3892/mmr.2019.10397
31. Rissman RA, Poon WW, Blurton-Jones M, et al. Caspase-cleavage of tau is an early event in Alzheimer disease tangle pathology. *J Clin Invest*. 2004;114(1):121–130. doi:10.1172/JCI20640
32. Sharma VK, Singh TG. CREB: a multifaceted target for alzheimer's disease. *Current Alzheimer Res*. 2020;17(14):1280–1293. doi:10.2174/1567205018666210218152253
33. Sobolczyk M, Boczek T. Astrocytic calcium and cAMP in neurodegenerative diseases. *Front Cell Neurosci*. 2022;16:889939. doi:10.3389/fncel.2022.889939
34. Bergantin LB. A timeline of Ca2+/cAMP signalling: from basic research to potential therapeutics for dementia. *Current Alzheimer Res*. 2022;19(3):179–187. doi:10.2174/1567205019666220415125447
35. Wang A, Bibb JA. Is CREB the angry bird that releases memory in Alzheimer's? *Neuropsychopharmacology*. 2011;36(11):2153–2154. doi:10.1038/npp.2011.126
36. Lonze BE, Ginty DD. Function and regulation of CREB family transcription factors in the nervous system. *Neuron*. 2002;35(4):605–623. doi:10.1016/s0896-6273(02)00828-0
37. Silva AJ, Kogan JH, Frankland PW, Kida S. CREB and memory. *Ann Rev Neurosci*. 1998;21:127–148. doi:10.1146/annurev.neuro.21.1.127
38. M.p M. Apoptosis in neurodegenerative disorders. *Nat Rev mol Cell Biol*. 2000;1(2):120–129. doi:10.1038/35040009
39. Ryu H, Lee J, Impey S, Ratan RR, Ferrante RJ. Antioxidants modulate mitochondrial PKA and increase CREB binding to D-loop DNA of the mitochondrial genome in neurons. *Proc Natl Acad Sci USA*. 2005;102(39):13915–13920. doi:10.1073/pnas.0502878102
40. Alausa A, Ogundepo S, Olaleke B, Adeyemi R, Olatinwo M, Ismail A. Chinese nutraceuticals and physical activity; their role in neurodegenerative tauopathies. *ChinMed*. 2021;16(1):1. doi:10.1186/s13020-020-00418-7